A new temperature-photoperiod coupled phenology module in LPJ-GUESS model v4.1: optimizing estimation of terrestrial carbon and water processes

Shouzhi Chen[1], Yongshuo H. Fu[1,2*], Mingwei Li[1], Zitong Jia[1], Yishuo Cui[1], Jing Tang[3*]

[1]College of Water Sciences, Beijing Normal University, Beijing 100875, China.

[2]Plants and Ecosystems, Department of Biology, University of Antwerp, Antwerp, Belgium.

[3] Center for Volatile Interactions, Department of Biology, University of Copenhagen, Denmark.

Corresponding author:

Yongshuo Fu (yfu@bnu.edu.cn); Jing Tang (jing.tang@bio.ku.dk).

Abstract

Vegetation phenological shifts impact the terrestrial carbon and water cycle and affect the local climate system through biophysical and biochemical processes. Dynamic Global Vegetation Models (DGVMs), serving as pivotal simulation tools for investigating climate impacts on terrestrial ecosystem processes, incorporate representations of vegetation phenological processes. Nevertheless, it is still a challenge to achieve accurate simulation of vegetation phenology in the DGVMs. Here, we developed and implemented spring and autumn phenology algorithms into one of the DGVMs, LPJ-GUESS. The new phenology modules are driven by temperature and photoperiod, and are parameterized for deciduous trees and shrubs by using remotely sensed phenological observations and the reanalysis data ERA5. The results show that

the LPJ-GUESS with the new phenology modules substantially improved the accuracy in capturing the start and end dates of growing seasons. For the start of the growing season, the simulated RMSE for deciduous trees and shrubs decreased by 8.04 and 17.34 days, respectively. For the autumn phenology, the simulated RMSE for deciduous trees and shrubs decreased by 22.61 and 17.60 days, respectively. Interestingly, we have also found that differences in the simulated start and end of the growing season also alter the simulated ecological niches and competitive relationships among different plant functional types (PFTs), and subsequentially influence the terrestrial carbon and water cycles. Hence, our study highlights the importance of accurate phenology estimation to reduce the uncertainties in plant distribution and terrestrial carbon and water cycling.

Keywords: LPJ-GUESS, phenology algorithm, model modification, ecological processes

1. Introduction

Vegetation plays a pivotal role within the terrestrial ecosystem, as the interplay between vegetation and climate exerts significant influence on the mass and energy cycles across a broad range of temporal and spatial scales (Zhu et al., 2016; Piao et al., 2019; Chen et al., 2022a). In recent years, with the increase of carbon dioxide concentration and land surface temperature, significant vegetation greening has been reported worldwide, and the annual growth dynamics of vegetation have undergone significant changes, especially the spring and autumn phenological changes (Zhu et al., 2016). A large amount of research evidence has indicated that climate change results in the advancement of spring phenology and the postponement of autumn phenology, exerting a profound influence on the carbon and water cycles within terrestrial ecosystems (Piao et al., 2019; Badeck et al., 2004; Zhou et al., 2020), and the geographic distribution of species (Chuine, 2010; Fang and Lechowicz, 2006; Huang et al., 2017). Under conditions of sufficient water supply and no radiation constraints, the extension of the growing season resulting from vegetation phenological shifts will contribute additional carbon sinks to terrestrial ecosystems (Zhang et al., 2020; Keenan et al., 2014). Longer growing seasons also lead to greater evapotranspiration, mainly in early spring and autumn, which in turn reduces watershed runoff (Huang et al., 2017; Kim et al., 2018; Chen et al., 2022b; Geng et al., 2020). Nevertheless, it is still a challenge to achieve accurate simulation of vegetation phenology in dynamic global vegetation models (DGVMs), especially in the context of climate change (Richardson et al., 2012). We urgingly caution that improving the vegetation phenology module of

DGVMs, and taking the response of vegetation phenology to climate change into consideration is a necessary development to improve model simulation accuracy and reduce model uncertainty.

The DGVMs generally include phenology modules in vegetation submodels, but the implementations vary widely, which include: 1) Using fixed and prescribed seasonal dynamics to characterize phenology, and the models using this method include SiB model, SiBCASA model, ISAM model, etc. (Sellers et al., 1986; Schaefer et al., 2008; Jain and Yang, 2005). 2) Using remote sensing data or in-situ observations directly describing the vegetation growth dynamics instead of process-based simulation, SiB2, BEPS and ED2 are all based on this method to describe the vegetation growth dynamics (Sellers et al., 1996; Deng et al., 2006; Medvigy et al., 2009). 3) Using vegetation phenology algorithm which take the response of vegetation biophysiology to environment factors into account to simulate vegetation growth dynamics. In comparison to the first two methods, the third approach offers the advantage of depicting the responses of vegetation to the external environment grounded in plant physiological process, and can trace the dynamics of vegetation growth amidst changing environmental conditions, so it is adopted by several DGVMs, e.g. Biome-BGC, ORCHIDEE and LPJ-GUESS (Thornton et al., 2002; Krinner et al., 2005; Sitch et al., 2003). With the evolving comprehension of the intricate response mechanisms of vegetation to external environment, vegetation phenological algorithms have experienced substantial advancements in recent decades, which encompass shifts from single-process to multi-process mechanisms and from single-variable to multi-factor

model constraints (Liu et al., 2018a; Fu et al., 2020; Piao et al., 2019). For spring phenological algorithms, in the early stage, temperature was the only factor considered, resulting in relatively simplistic model processes, which were also commonly adopted by DGVMs (GDD and Unified, etc.) (Sarvas, 1972; Chuine, 2000). With the deepening of the understanding of spring phenological mechanisms, factors such as radiation and photoperiod have been introduced into the phenological algorithm, and the corresponding complex regulatory mechanisms have also been perfected, e.g. Sequential algorithm, Parallel algorithm and DORMPHOT algorithm (Hänninen, 1990; Kramer, 1994; Caffarra et al., 2011). As for the autumn phenological algorithm, the early algorithm form was also relatively simple (cold temperature-driven CDD algorithm) but widely used in DGVMs, and some DGVMs used fixed leaf longevity for the determination of autumn phenological dates. The development of relatively complex autumn phenological mechanism algorithms is relatively late, and these advanced autumn phenological algorithms take photoperiod and carbon accumulation into account in the algorithm process, such as temperature-photoperiod bioclimatic (DM) algorithm, photosynthesis-influenced autumn phenology (PIA) algorithm (Zani et al., 2020; Delpierre et al., 2009). Many studies have pointed out that early phenological algorithms tend to be overly simplistic and result in biased predictions, which indicates that the vegetation phenological algorithms of DGVMs need to be updated urgently (Kucharik et al., 2006; Ryu et al., 2008). The use of more accurate phenological algorithms covering more complex mechanisms is of great significance in reducing the simulation errors of DGVMs and improving the simulation reliability

under future climate warming.

In this study, we used the remote sensing-based phenology data and the threshold and maximum change rate methods to parameterize the spring DORMPHOT algorithm and autumn DM algorithm. This was explicitly applied for boreal needle-leaved summergreen tree (BNS), Shade-intolerant broadleaved summergreen tree (IBS), shade-tolerant temperate broadleaved summergreen tree (TeBS) and summergreen shrubs plant function types (PFTs). The new phenology module with these parameters was coupled into the LPJ-GUESS model. The objectives of this study are as follows: 1) to couple more mechanistic phenology modules into LPJ-GUESS to improve the accuracy of spring and autumn phenology simulations; (2) to assess the impacts of different vegetation phenological algorithms on the carbon and water process simulations.

2. Materials and methods

2.1 Datasets

2.1.1 GIMMS $NDVI_{4g}$

Normalized differential vegetation index (NDVI) is commonly used as a proxy for vegetation canopy greenness and growth condition. In the study, we used the fourth-generation NDVI dataset of GIMMS, which provides biweekly NDVI records with a spatial resolution of 1/12° (~8 km) during 1982-2017 to extract the start and end of growing season (Pinzon and Tucker, 2014; Tucker et al., 2005; Cao et al., 2023). This NDVI dataset has been refined and corrected for orbital drift, calibration, viewing

geometry, and volcanic aerosols, which can accurately reflect the accurate growth dynamics of surface vegetation (Kaufmann et al., 2000).

2.1.2 Climate forcing field data

We used CRU-NCEP V7 data with a horizontal spatial resolution of 0.5° × 0.5° as the forcing field data for driving the LPJ-GUESS model during 1901-2015. The forcing field data include monthly air temperature (1901-1978) and precipitation, wind speed, wet days, incoming shortwave radiation and relative humidity over the period 1901-2015, which can be downloaded from https://rda.ucar.edu/datasets/ds314.3/. The ERA5-Land daily air temperature dataset has been used to parameterize spring and autumn phenological algorithms and force LPJ-GUESS model. The dataset is a global reanalysis dataset developed by the European Centre for Medium-Range Weather Forecasts (ECMWF), which utilises advanced data assimilation techniques combining observations from various sources, such as satellites, weather stations, and weather balloons, with numerical weather prediction models. We downloaded the ERA5 land daily air temperature at 0.5° spatial resolution (consistent with CRU NCEP V7 data, from 1979-2015) from their official website (https://cds.climate.copernicus.eu/cdsapp#!/dataset/reanalysis-era5-land?tab=form). Due to possible bias between different data sets, we calculated the monthly average of ERA5 land daily air temperature and calculated its climatology, as well as the climatology of CRU NCEP v7 monthly air temperature data, and corrected the bias of ERA5 land data according to the deviation.

2.1.3 GLC 2000 land cover data

Satellite remote sensing can capture the collective information from mixed pixels comprised of various plants and also information from dominant vegetation. The data acquired through satellite remote sensing can be regarded as representative of a particular vegetation type only when the plant functional types within a gridcell exhibit a relatively homogeneous composition. Based on GLC2000 land cover types data, which are designated according to PFTs ascribed to satellite images and ground truth by regional analysts with 1 km spatial resolution (Bartholome and Belward, 2005), we calculated the proportion of different PFTs in the 0.5°×0.5° gridcell to identify pixels dominated by a specific plant functional type (the proportion of a specific plant function type is greater than 50%, Fig. 1 and Fig. S1).

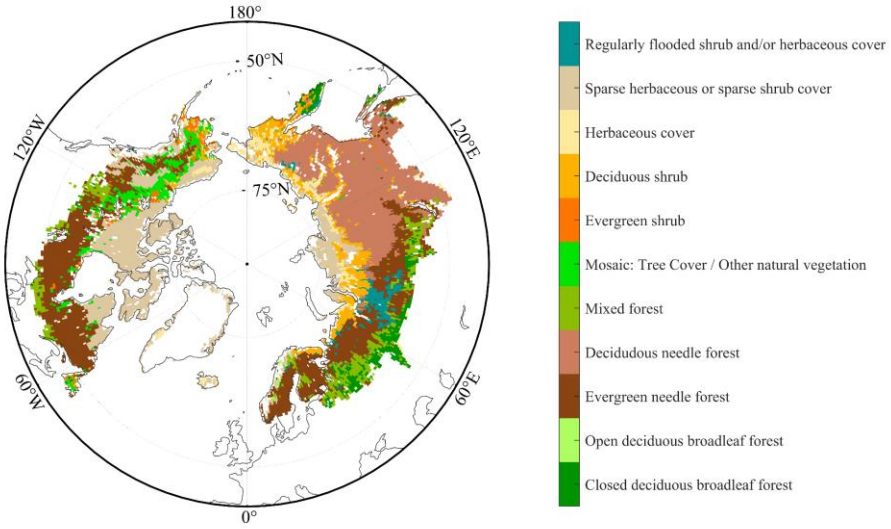

Figure 1. **The spatial distributions of 11 detailed regional land-cover types in the GLC2000 products.** BNS (boreal needle-leaved summergreen tree): Deciduous needle forest, IBS&TeBS (Shade-intolerant broadleaved summergreen tree and shade-tolerant temperate broadleaved summergreen tree): Open deciduous broadleaf forest and closed deciduous broadleaf forest, Shrubs (summergreen shrubs): Sparse herbaceous or sparse shrub cover and Deciduous shrub.

2.1.4 VPM GPP and REA ET data

We used the vegetation photosynthesis model (VPM) gross primary productivity (GPP) (Zhang et al., 2017) and REA ET (Lu et al., 2021) to compare the simulation results of carbon and water fluxes with the LPJ-GUESS model.

The VPM GPP dataset is constructed upon an enhanced light use efficiency theory, utilizing satellite data from MODIS and climate data from NCEP Reanalysis II. It incorporates an advanced vegetation index (VI) gap-filling and smoothing algorithm, along with distinct considerations for C3/C4 photosynthesis pathways. VPM GPP product can be downloaded from https://data.nal.usda.gov/dataset/global-moderate-resolution-dataset-gross-primary-production-vegetation-2000%E2%80%932016.

ERA ET is a combination of three existing model-based products – the fifth-generation ECMWF reanalysis (ERA5), Global Land Data Assimilation System Version 2 (GLDAS2), and the second Modern-Era Retrospective analysis for Research and Applications (MERRA-2), which uses the reliability ensemble averaging (REA) method, minimizing errors using reference data, to combine the three products over regions with high consistencies between the products using the coefficient of variation (CV). The REA ET data can be accessed at https://doi.org/10.5281/zenodo.4595941 (Lu et al., 2021).

2.2 Phenology dates extraction

We used five phenological extraction methods, which include three threshold-based methods (i.e. Gaussian-Midpoint, Spline-Midpoint and Timesat-SG Methods) and two change rate-based methods (i.e. the HANTS-Maximum and Polyfit-Maximum

methods) following previous studies (Cong et al., 2012; Savitzky and Golay, 1964; Chen et al., 2023), to retrieval spring (start of growing season, SOS) and autumn (end of growing season, EOS) phenological events (Fig.S2). Phenological extraction based on multiple methods consists of three steps: 1) smoothing and interpolating the NDVI date to obtain the smooth and continuous NDVI daily time series; 2) using the threshold value (0.5 for SOS and 0.2 for EOS) or the maximum rate of change to extract the vegetation phenology from each single method (Reed et al., 1994; White et al., 1997; White et al., 2009; Piao et al., 2006); 3) averaging the phenological results obtained by different extraction methods to reduce uncertainties associated with a single method (Due to the different fitting methods, interpolation methods and threshold settings of different extraction methods) (Fu et al., 2021; Fu et al., 2023).

2.3 Model description

LPJ-GUESS is a process-based dynamic global vegetation model that can simulate vegetation dynamics and soil biogeochemical processes across different terrestrial ecosystems. At the gridcell level, the model simulates vegetation growth, allometry competition, mortality and disturbances (Sitch et al., 2003; Morales et al., 2005; Hickler et al., 2004). The PFTs within the framework of the LPJ-GUESS model encapsulate the extensive spectrum of structural and functional attributes characteristic of potential plant species. Within a given area (patch, corresponding in size approximately to the maximum area of influence of one large adult individual on its neighbors), plant growth is governed by the synergistic interplay of bioclimatic constraints and interspecific competition for spatial dominance, access to light, and

vital resources. In a gridcell (stand), it's typically simulating multiple such patches to represent different disturbance histories within a landscape, and across these patches, the modeled properties tend to coalesce towards a singular, overarching average value (Smith et al., 2001).

In LPJ-GUESS model, spring phenology is calculated based on spring heat and winter cold requirements (Sykes et al., 1996). Plants have certain energy requirements for budburst, which are expressed by using growing degree days above 5 degrees (GDD5), while growing degree days to budburst is also related to the length of the chilling period. An increase in chilling periods can reduce the requirement for growing degree days to budburst, in other words, budburst can be delayed long enough to minimize the risk that the emerging buds will be damaged by frost (Equation 1):

$$GDD = a + b \times e^{-k \times C} \quad (1)$$

Where a, b and k are PFT-specific constants, and C is the length of chilling period. GDD represents the growing degree days requirement of a specific PFT at a chilling period length of C. Growing degree days are defined as the accumulation of temperatures above the base temperature (generally 5 ℃), and the length of chilling period is defined as the days that daily mean temperature below 5 ℃.

For autumn phenology, leaf longevity was used as a threshold in the LPJ-GUESS model for the simple prediction of senescence. It is assumed in the model that autumn phenology occurs when the cumulative complete leaf longevity is greater than 210 days or the daily average temperature below 5℃ in autumn.

Within each stand, 50 different patches (in this study) were applied to represent different disturbance histories within a landscape. The simulations over the study areas included 23 PFTs, which consist of five grass, three bryophytes, eight shrubs and seven tree PFTs, and the summergreen PFTs involved in the improvement of vegetation phenological simulation contain BNS, IBS, TeBS and deciduous shrubs (hereafter called Shrubs), see detailed description in (Tang et al., 2023) and Rinnan et al. (2020).

2.4 LPJ-GUESS phenology module extension

We improved the spring and autumn phenological modules of the LPJ-GUESS model by coupling DORMPHOT algorithm and DM algorithm into LPJ-GUESS according to the phenological module extension flow chart (Fig.2).

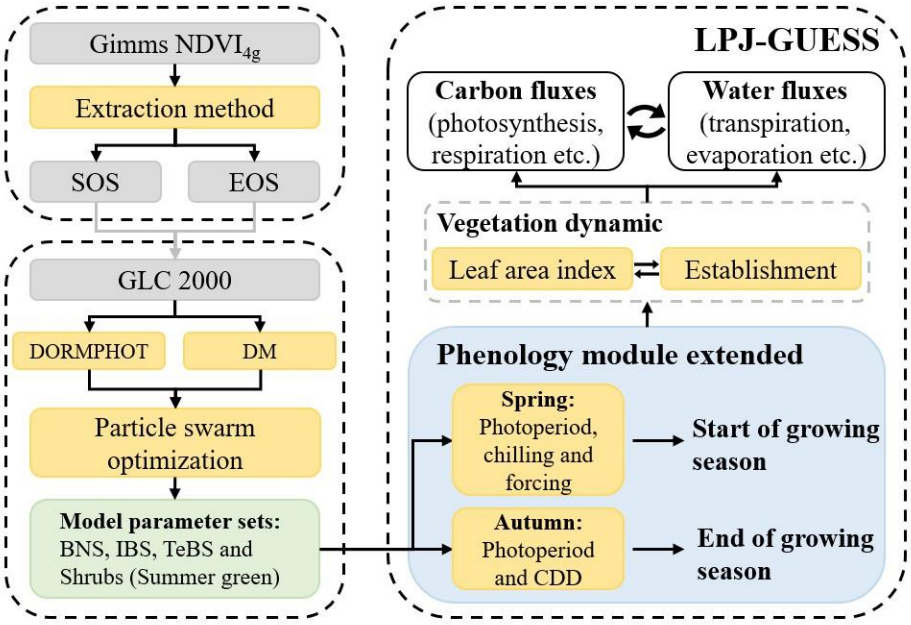

Figure 2 Flowchart of spring and autumn phenological module extension in LPJ-GUESS. Dotted boxes represent independent work, gray boxes represent different data sets or intermediate process results, and yellow boxes represent different calculation methods or model modules. CDD, cold degree days.

The spring phenological algorithm in LPJ-GUESS was replaced by DORMPHOT algorithm, which introduces the effect of photoperiod on dormancy. This algorithm refines the spring phenological algorithm into three stages: dormancy induction, dormancy release and growth resumption (Caffarra et al., 2011). The dormancy induction process is triggered by a short photoperiod (DR_P) and a low temperature (DR_T), and finishes when the cumulant of the product of DR_P and DR_T reaches a specific threshold ($DS > D_{crit}$, Equation 2, 3 and 4):

$$DS = \sum_{t_0}^{t} DR_T \times DR_P \tag{2}$$

$$DR_T = \frac{1}{1+e^{aD\times(T-bD)}} \tag{3}$$

$$DR_P = \frac{1}{1+e^{10\times(DL-DL_{crit})}} \tag{4}$$

Where t_0 is the start date of dormancy induction, which defined at September 1st of the year preceding budburst, DS represents the state of dormancy induction (the cumulant of daily photoperiod, i.e. DR_P, and temperature, i.e. DR_T, effect), T is the daily mean temperature, and DL is day length on day t. aD, bD and DL_{crit} are algorithm parameters that regulate the effect of photoperiod and temperature.

Dormancy release and growth resumption start after dormancy induction is complete (t_d), which represent a parallel chilling and forcing process, respectively. The total daily rate of chilling (S_C) is defined as the accumulation of daily chilling (R_C) as

Equation 5, and the daily forcing (R_f) is determined by both photoperiod and S_C (Equation 6, 7 and 8), that the effect of photoperiod and chilling on R_f counteracts each other. The increase of photoperiod will decrease R_f while the increase of chilling will reverse the effect:

$$S_C = \sum_{t_d}^{t} R_C = \sum_{t_d}^{t} \frac{1}{1 + e^{aC \times (T\text{-}cC)^2 + (T\text{-}cC)}} \tag{5}$$

$$DL_{50} = \frac{24}{1 + e^{hDL \times (S_C - C_{crit})}} \tag{6}$$

$$T_{50} = \frac{60}{1 + e^{gT \times (DL - DL_{50})}} \tag{7}$$

$$S_f = \sum_{t_d}^{t} R_f = \sum_{t_d}^{t} \frac{1}{1 + e^{dF \times (T - T_{50})}} \tag{8}$$

Where aC, cC and C_{crit} are the algorithm parameters of chilling process, and hDL, gT and dF are the algorithm parameters of forcing process. When the total daily rate of forcing (S_f) reaches a critical value F_{crit}, vegetation completely resumes growth and spring phenological events occurred. Note that gT and hDL must be greater than zero to limit the monotonicity of Equation 6 and 7.

Since the lack of process based submodule to simulate autumn phenology in LPJ-GUESS model, and only a fixed leaf longevity is used to define occurrence date of autumn phenology, we introduced autumn phenology process that considers photoperiod and cold temperature effects by coupling the DM algorithm into the LPJ-

GUESS model (Delpierre et al., 2009). The DM algorithm assumes that plants will respond to low temperature (below base temperature, T_b) only when the photoperiod is below a critical value (DL_{crit}), and the daily rate of senescence (R_{sen}) on that day is determined by cold temperature and photoperiod (Equation 9,10 and 11):

$$f(DL) = \alpha_{pn} \times \frac{DL}{DL_{crit}} + (1-\alpha_{pn}) \times \left(1 - \frac{DL}{DL_{crit}}\right), \ \alpha_{pn} \in \{0,1\} \tag{9}$$

$$R_{sen} = \begin{cases} 0, & DL \geq DL_{crit} \\ 0, & DL < DL_{crit} \ \& \ T \geq T_b \\ (T_b - T)^x \times f(DL)^y, & DL < DL_{crit} \ \& \ T < T_b \end{cases} \tag{10}$$

$$S_{sen} = \sum_{t_0}^{t} R_{sen} \tag{11}$$

Where α_{pn} is a parameter determines that photoperiod shorter than the DL_{crit} threshold weaken (α_{pn} equal to 1) or strength (α_{pn} equal to 0) the cold-degree sum effect. x and y are the indices of the temperature and photoperiod terms in the formula, which are used to adjust the degree of influence of temperature and photoperiod on Rsen, respectively.

2.5 Phenological algorithm parameterization

Utilizing the spatial distribution of predominantly homogeneous pixels corresponding to distinct vegetation types, we partitioned the remote sensing phenological dataset, and finally obtained the phenological dataset of BNS, IBS, TeBS and Shrubs for the parameterization of DORMPHOT and DM algorithms. We divided the phenology dataset into two parts according to the odd or even number of years, the

odd-numbered years for algorithm parameter internal calibration and the even-numbered years for algorithm external calibration. Particle swarm optimization (PSO) algorithm was applied to parameterize the DORMPHOT and DM algorithm for different PFTs, which used the mixed function that comprehensively considers multiple evaluation indicators as the objective function ($f(mixed)$, Equation 12), and sets the upper limit of iteration to 5000 times to find the global optimal parameter (Marini and Walczak, 2015; Poli et al., 2007). The parameters of DORMPHOT algorithm and DM algorithm applicable to BNS, IBS&TeBS and Shrubs PFTs were found by PSO algorithm (Table S1 and S2).

$$f(mixed) = 100 \times (1 - R^2) + 100 \times (1 - NSE) + 10 \times RMSE \quad (12)$$

Where R^2 is coefficient of determination, NSE is Nash–Sutcliffe Efficiency, and RMSE is Root mean square error. The coefficients in front of each term of the formula are used to adjust the weights of different evaluation indicators. The smaller the objective function, the closer the simulated value of the algorithm is to the observed value.

2.6 Simulation set-up

To compare the simulation performance of LPJ-GUESS which employing original phenological module and modified phenological module (the extended LPJ-GUESS). We first ran the model using CRU NCEP v7 gridded climate data over the period 1901-1978 with a 500 year spin up, and saved all model state variables at the end of 1978 (used the original phenological module, and the status variables associated with the

307 extended phenological module were also updated and saved concurrently). Avoiding
308 the differences in the simulated vegetation and soil state variables outside the study
309 period, i.e. 1979-2015 (Viovy, 2018). Then we restarted the model simulations
310 (applying the original phenological module and extended phenological module,
311 respectively) with the saved model state variables at the last day of 1978 and ERA5
312 land daily air temperature; note that other forcing data were still from CRU NCEP v7
313 data set, and printed start (end) of growing season of summer green PFTs, monthly grid
314 level GPP and actual evapotranspiration (AET) of each PFT and foliar projection cover
315 (FPC), for investigating the simulation difference which induced by phenological
316 simulation differences. All the data processing and analysis in this study were
317 completed in Matlab 2020b (www.mathworks.com).

318

319 **3. Results**

320 **3.1 Phenology simulation performance**

321 For spring phenology, DORMPHOT algorithm has the best simulation
322 performance in the IBS&TeBS region (R^2 = 0.62 & NSE = 0.62), followed by in the
323 regions dominated by BNS (R^2 = 0.52 & NSE = 0.52) and Shrubs (R^2 = 0.47 & NSE =
324 0.47) (Table 1). For autumn phenology, the simulation performance was generally
325 worse than that of spring phenology. The DM algorithm has the best simulation
326 performance in the Shrubs region, (R^2 = 0.39 & NSE = 0.39), followed by the regions
327 dominated by BNS (R^2 = 0.33 & NSE = 0.32) and IBS&TeBS (R^2 = 0.47 & NSE =

328 0.47) (Table 1).

329 **Table 1** Algorithm **performances of DORMPHOT and DM** algorithm**s.**

Algorithm	Plant function type	Internal calibration			External calibration		
		R^2	*NSE*	*RMSE*	*R^2*	*NSE*	*RMSE*
DORMPHOT	BNS	0.54	0.53	7.71	0.52	0.52	7.96
	IBS&TeBS	0.61	0.61	7.92	0.62	0.62	7.91
	Shrub	0.45	0.44	11.3	0.47	0.47	11.1
DM	BNS	0.28	0.28	10.7	0.33	0.32	10.7
	IBS&TeBS	0.29	0.28	14.9	0.32	0.31	14.4
	Shrub	0.42	0.42	10.4	0.39	0.39	10.5

330 R^2, coefficient of determination, NSE, Nash–Sutcliffe Efficiency, RMSE, Root mean
331 square error. BNS, boreal needle-leaved summergreen tree, IBS, Shade-intolerant
332 broadleaved summergreen tree, TeBS, shade-tolerant temperate broadleaved
333 summergreen tree and Shrubs, summergreen shrubs plant function types**.**
334

335 Compared with remote sensing-based vegetation phenological indices, LPJ-
336 GUESS with the original phenological module estimated earlier spring onset and
337 autumn leaf senescence. The simulated spring phenology matches better than that of
338 autumn phenology. The extended LPJ-GUESS model has greatly improved the
339 estimation accuracy in regions dominated by BNS, IBS&TeBS and Shrubs PFTs (Fig.
340 3 and Fig. S3). For spring phenology, the simulated R^2 (RMSE) of the extended LPJ-
341 GUESS model for regions dominated by BNS, IBS&TeBS and Shrubs PFTs were 0.53
342 (7.84), 0.61 (7.92) and 0.46 (11.21), respectively, which increased (decreased) by 0.26
343 (5.55), 0.12 (17.34) and 0.25 (10.53) compared with the original phenological module.

344 We found that PFTs with larger R^2 increases in spring phenological simulation also
345 had smaller RMSE reductions for the extended model, indicating the improvements in
346 capturing interannual change and the multi-year mean value. The autumn phenology

simulation performance was greatly improved by integrating DM algorithm for regions dominated by BNS, IBS&TeBS and Shrubs PFTs, the simulated R^2 (RMSE) of the extended LPJ-GUESS model were 0.31 (10.70), 0.31 (14.69) and 0.41 (10.42), respectively, which increased (decreased) by 0.11 (15.66), 0.31 (17.60) and 0.27 (27.50). By comparing the LPJ-GUESS simulated daily LAI before and after coupling the DM algorithm, we also found that the autumn LAI values simulated by the extended LPJ-GUESS no longer suddenly decrease to 0 over a day but rather smoothly decrease with the sigmoid function according to the control of cold temperature and photoperiod (Fig. S4).

We also used two calibration schemes to explore the phenology simulation performance of the original phenological module of LPJ-GUESS after parameterization. The first one is based on the original LPJ-GUESS model to determine a common parameter set of all deciduous tree PFTs, and the second one is to determine a unique set of parameters for each PFTs. The results show that the phenology simulation performance of the original phenological module under the two calibration schemes was inferior to that of the new phenological module based on the cooperative control of temperature and photoperiod (Table S3)

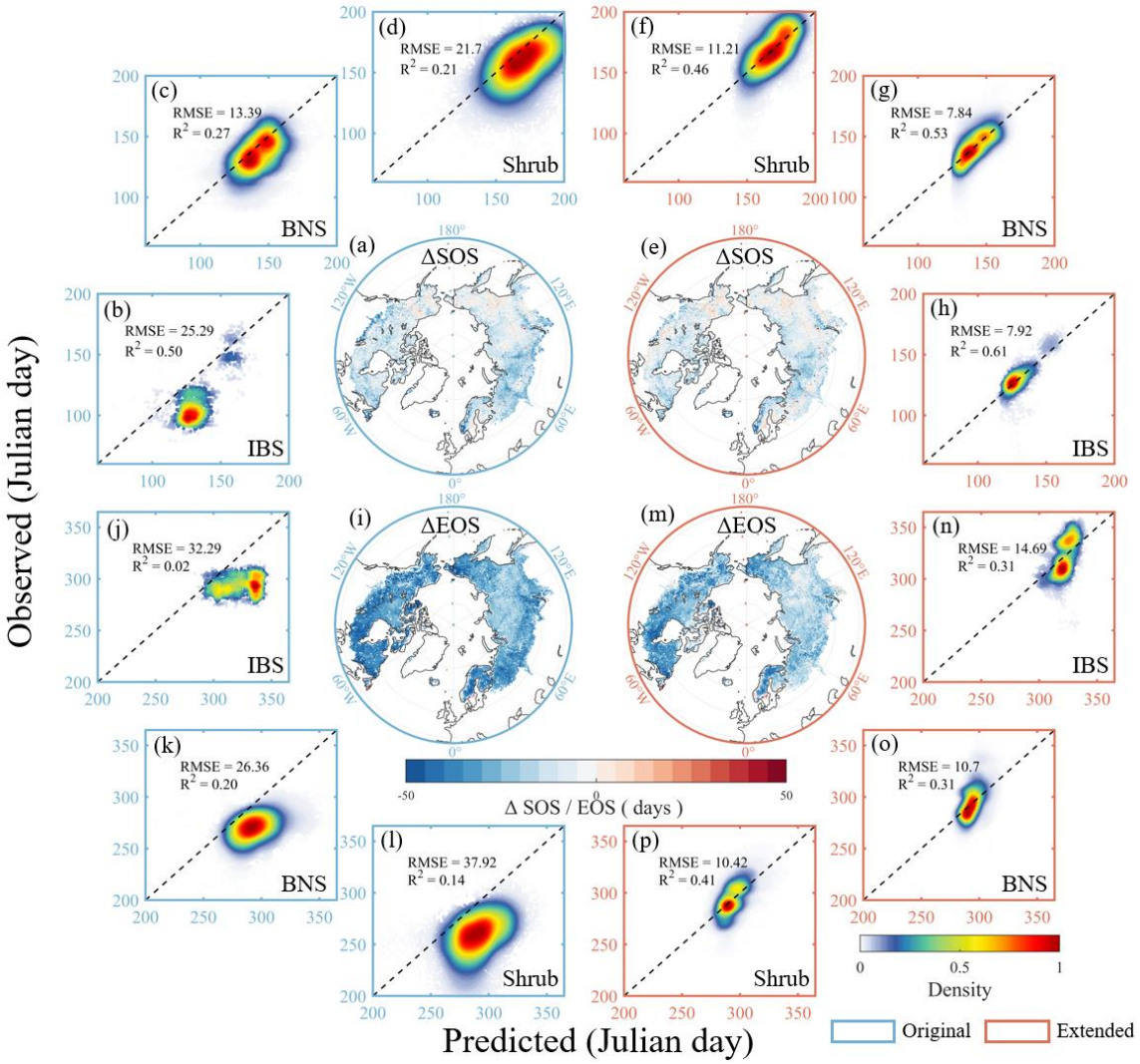

Figure 3 Comparison of the simulated performance of spring (SOS) and autumn (EOS) phenology between the original (left blue panels) and the extended (right red panels) LPJ-GUESS. (a-d) Simulation performance of SOS using the original LPJ-GUESS, (e-h) Simulation performance of SOS using the extended LPJ-GUESS, (i-l) Simulation performance of EOS using the original LPJ-GUESS, (m-p) Simulation performance of EOS using the extended LPJ-GUESS. Blue and red boxes represent spring and autumn phenological simulations. The spatial geographic map showed the difference between the simulation results of LPJ-GUESS model and the remote sensing phenology, with blue representing the model underestimation and red representing the model overestimation. The dotted lines in the subgraph are 1:1 lines.

3.2 Gross primary productivity simulation

Since the PFTs simulated in the LPJ-GUESS model include not only BNS, IBS&TeBS and Shrubs, but also evergreen plants and grass (no development was made to its phenological simulation in the present study), we found that clear differences

between two versions of the model mainly appeared in the regions dominated by these deciduous PFTs with improved phenological modules. We only found small differences in the regions dominated by evergreen or grassland (Fig. 4c). It is also clear that the original LPJ-GUESS generally simulated higher GPP than the extended one over the study period, except for the IBS&TeBS dominated regions, where higher GPP from the original model can be only found from 1979 to 2000 (Fig. 4d-f). By comparing multiple years' monthly mean GPP values, it becomes evident that the extended phenology also influences the seasonal dynamics of GPP. In regions dominated by BNS, the differences in monthly GPP are primarily noticeable during spring (using extended phenological module resulted in a -34.9% lower GPP in May compared to original phenological module, when not specifically stated, the value is that the extended model differs from the original model, Fig. 4g). In regions dominated by IBS&TeBS, GPP differs in both spring (-2.8%) and autumn (-6.3%) and the difference is larger in autumn, which mainly contribute to annually GPP difference (Fig. 4h). In Shrubs dominate regions, we found differences in GPP in all months (-43.9%), especially in the non-growing season, indicating that some evergreen plants still exist in the region when the original phenological module is used, and that changes in vegetation phenology seems substantially affect vegetation composition in this region (Fig. 4i). Compared with VPM GPP products, we also found that LPJ-GUESS simulated GPP overestimate but spatial pattern is consistent with VPM GPP products and extended LPJ-GUESS model could simulate GPP more accurately during transition periods (Fig. S5 and S6).

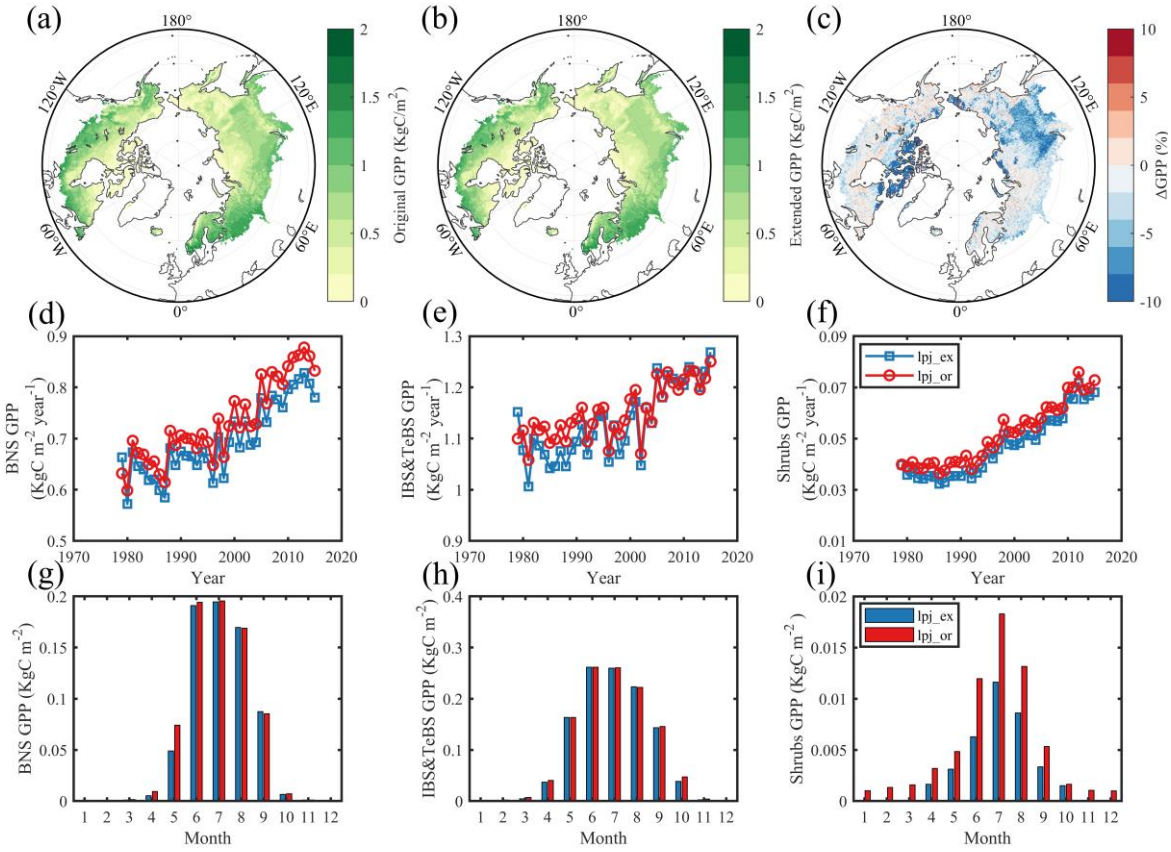

Figure 4 Comparison of gross primary productivity (GPP) simulations between scenarios which used the original phenological module and extended (DORMPHOT and DM) phenological module. (a) The scenario used the original phenological module, (b) The scenario used the extended phenological module, and (c) the difference between the two scenarios mentioned above, blue represents a larger simulation value for the LPJ-GUESS model using the original phenological module, and red is smaller. (d-f) Annual average GPP for BNS, IBS&TeBS and Shrubs PFTs from 1979 to 2015. (g-i) Multi-year mean monthly GPP for BNS, IBS&TeBS and Shrubs PFTs from 1979 to 2015.

The potential natural plant distribution also confirmed that the gridcells with large differences in phenological simulations between original and the extended LPJ-GUESS also has large differences in dominant vegetation types (Fig. S3). We selected typical gridcells in BNS, IBS&TeBS and Shrubs regions, and compared their multi-year variation pattern of FPC. We found that phenological changes had a clear influence on FPC changes in BNS and Shrubs region (Fig. 5). However, in the IBS&TeBS region

(the gridcell dominated by IBS was selected here), although we found that the difference in phenological simulation effects little on FPC components, due to the close proportion of IBS and BNE (fierce competition), small changes in FPC components could also lead to changes in dominant vegetation types (Fig. 5c, d).

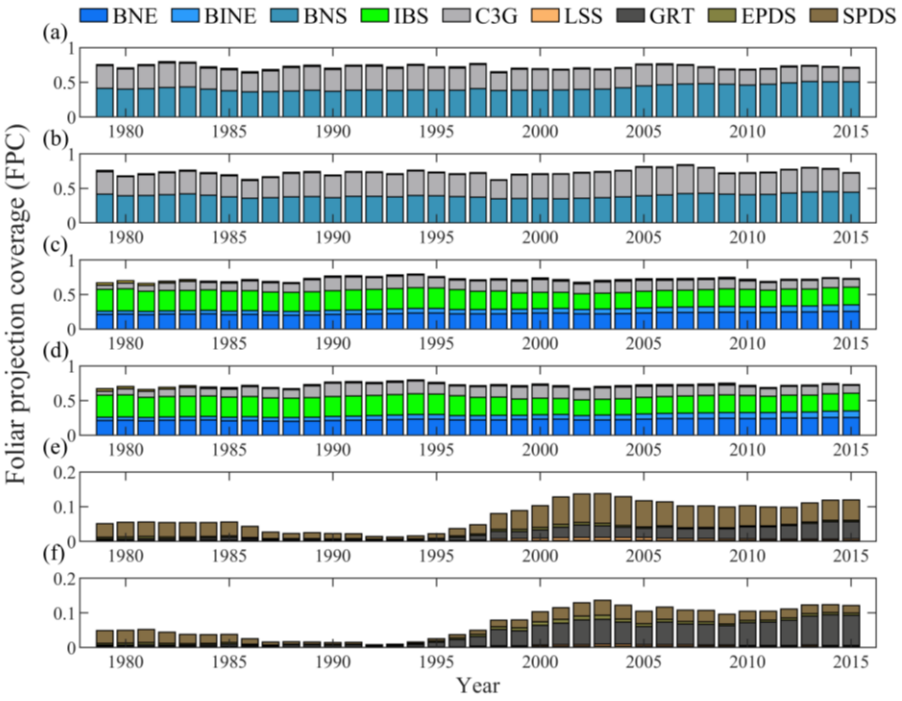

Figure 5. Shifts of foliage projection coverage (FPC) of typical gridcell in the regions dominated by BNS, IBS & TeBS and Shrubs PFTs over the period 1979 - 2015. (a) BNS, (c) IBS&TeBS and (e) Shrubs typical gridcells used original LPJ-GUESS model, (b) BNS, (d) IBS&TeBS and (f) Shrubs typical gridcells used extended LPJ-GUESS model.

3.3 Evapotranspiration simulation

By comparing the spatial pattern, we found that LPJ-GUESS simulated AET spatial pattern is consistent with REA ET products and BNS dominated the regions with large differences in the modelled AET under the two runs, and the simulation result using the original phenological module were larger by 3.9% compared with that using the modified module (Fig.6c and S7). In the IBS&TeBS dominated region, like GPP,

we found that the scenario using the original phenological module presented a larger AET during the period 1979-2000, and the two scenarios simulated AET in the Shrubs dominated region were very close (Fig. 6e-f). The seasonal dynamic patterns of AET in BNS, IBS&TeBS and Shrubs-dominated regions are similar. The AET simulations get higher in spring and lower in summer, and only in the Shrubs-dominated region, the AET simulation get lower in autumn when the original phenology module is used (Fig. 6g-i).

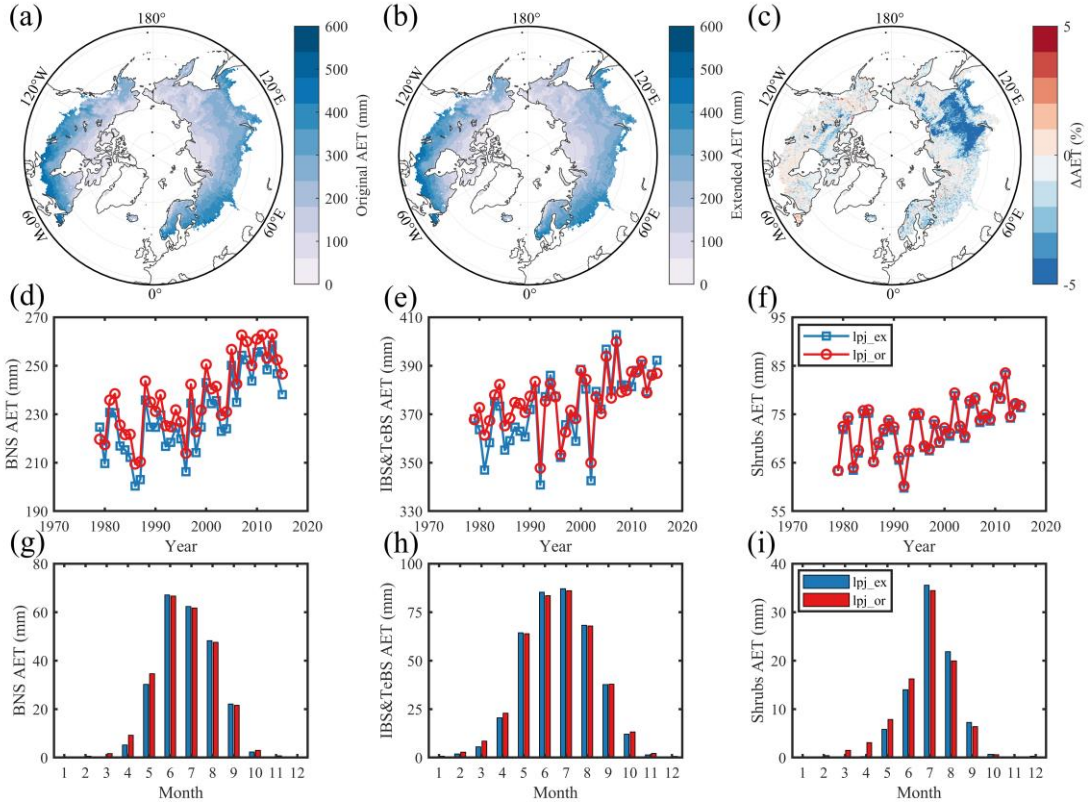

Figure 6 Comparison of actual evapotranspiration simulations between scenarios which used original phenological module and extended (DORMPHOT and DM) phenological module. (a) Scenario used original phenological module, (b) scenario used extended phenological module, and (c) the difference between the two scenarios mentioned above, blue represents a larger simulation value for the LPJ-GUESS model using the original phenological module, and red is smaller. (d-f) Annual average AET for BNS, IBS&TeBS and Shrubs PFTs from 1979 to 2015. (g-i) Multi-year mean monthly AET for BNS, IBS&TeBS and Shrubs PFTs from 1979 to 2015.

4. Discussion

4.1 Remote Sensing Phenology Facilitates Mixed-Pixel Phenology Modeling

Whether through dynamic global vegetation model simulation or satellite remote sensing extraction, a key issue in large-scale vegetation phenology research is the scale transformation of phenology data in mixed pixels. For phenological extraction based on satellite remote sensing, which is a top-down approach, the spring phenology extracted from the mixed pixel (without specific dominant vegetation types) is the information about the dates when the earliest plant leaf-out occurs in the pixel, while the autumn phenology is the last one to senescence (Chen et al., 2018; Reed et al., 1994; White et al., 2009; Fu et al., 2014). Furthermore, previous studies also have detected temporal lags between the phenology of NDVI, LAI and GPP, especially in tropical regions, where the saturation of optical vegetation indices, such as NDVI and LAI can limit the extraction of phenology, while SIF (solar-induced chlorophyll fluorescence) data could overcome this issue (Guan et al., 2015; Li et al., 2021; Hmimina et al., 2013). In addition, the greenness of understory phenology (low shrub or grass in forests) further complicates the detection of overstory signals (Ahl et al., 2006; Tremblay and Larocque, 2001). It is challenging to separate remote sensing signals into different components by filtering or decoupling methods. The more feasible method is to detect phenological changes with a few mixed species at a small spatial scale and conduct climate-controlled experiments (Wolkovich et al., 2012).

DGVM-based phenological simulation is based on a bottom-up method, different

from phenological extraction based on remote sensing. Many studies have investigated phenological algorithms based on remote sensing data, and ignored the influence of mixed pixels (Keenan and Richardson, 2015; White et al., 1997), which lacks extensibility and robustness under changing circumstances, e.g. climate change. DGVMs through simulating plant individuals' growth, development and senescence in the gridcell, which represents different signals in the mixed pixels, and finally synthesizes the vegetation signals of the whole gridcell (Sitch et al., 2003). In this study, based on top-down remote sensing phenology and parameter calibrations for several relatively pure pixels with a clear dominance of BNS, IBS&TeBS and Shrubs PFTs, we integrated this newly calibrated phenology module at PFT level into the LPJ-GUESS to reproduce the gridcell-level vegetation phenology for the mixed pixels. The simulation of vegetation phenology for mixed pixels enables the capture of phenological variability arising from dynamic vegetation changes, as opposed to the predefined approach reliant on specific pixel vegetation types, which also partly explains why phenological algorithms based on predefined vegetation types are difficult to generalize spatially (Chen et al., 2018). Leveraging the advantages of wide-ranging remote sensing phenological monitoring and stable monitoring frequencies, analyzing the relationship between pixel constituents and vegetation signals, especially in cases where pixel constituents are relatively uniform, can enhance the accuracy of phenological simulation for mixed pixels.

4.2 Influence of phenological shifts on ecosystem structure

Our results showed that LPJ-GUESS model, which using the original phenological

module estimated earlier SOS in BNS, IBS&TeBS and Shrubs dominant regions than that using the extended phenological module (Fig.3). Earlier spring phenology, which is closely related to plant growth and development and has a strong influence on interspecific competition (Roberts et al., 2015; Rollinson and Kaye, 2012), also lead to a larger dominant area (Fig. S3). In the high latitude regions, plants gain a competitive niche through the advancement of spring phenology if there is no damaged tissue and shoots induced by late frost and the weight of late snowfall (Augspurger, 2009; Bigler and Bugmann, 2018; Drepper et al., 2022; Liu et al., 2018b). This advancement is mediated by the early snowmelt synergistic changes of soil temperature and soil water content. It manifested in a wider window of high resource availability and low competition (Zheng et al., 2022). During this window period, plants can get more light, water and nutrient resources, and then carry out vegetative growth earlier, and finally increase the leaf area in the spring. As the community develops, changes in competitive relations at the species or functional group level in the spring will induce to changes in community composition (Morisette et al., 2009; Forrest et al., 2010). In the context of climate change, differences in the phenological responses of different species may further affect the distribution of species, and the inaccuracy of future phenological dynamic simulations of different vegetation types in DGVMs will introduce great uncertainty to the estimation of future potential natural plant distribution (Dijkstra et al., 2011), which further impacting GPP simulations, a key source of uncertainty for terrestrial carbon cycle simulations (Ahlström et al., 2015).

4.3 Further development of phenological algorithms

Although we have substantially improved the LPJ-GUESS' accuracy of simulating vegetation phenology by coupling calibrated spring (DORMPHT) and autumn (DM) phenological algorithms at PFT levels, we still see the discrepancy in the grass-dominated regions, which, owing to we did not employ the temperature and photoperiod phenological algorithm for grassland phenology simulation, because many studies indicate that grassland phenology is also regulated by precipitation (Fu et al., 2021). Furthermore, the current phenology algorithms only consider the synergistic effects of temperature and photoperiod, but can be further linked to plant growth and physiology (Fu et al., 2020; Zohner et al., 2023). In different regions (under different external conditions), the driving mechanism and effective driving factors of vegetation phenology process can be different. Temperature is an important factor regulating phenology in energy-limited regions, while water supply (precipitation, soil moisture, etc.) control cannot be ignored in water-limited regions (Prevéy et al., 2017; Fu et al., 2022). For further developing phenological modules in DGVMs, on the one hand, it is necessary to carry out mechanism research of phenology of different species through controlled experiments, to the end of improving the existing mechanism algorithm. On the other hand, it is necessary to introduce new methods, such as machine learning, for the accurate generalization of some complex key nonlinear processes (Fu et al., 2020; Dai et al., 2023). Through the above two aspects of work, a comprehensive phenological module can be provided for further improving the accuracy of DGVM models in simulating the phenological dynamics of different PFTs in different environments.

5. Conclusion

In this study, we parameterized and constructed spring (DORMPHOT) and autumn (DM) phenology algorithms for BNS, IBS&TeBS and Shrubs PFTs based on the remote sensing-extracted phenology data. These parameterized DORMPHOT and DM algorithms were further coupled into the LPJ-GUESS model, and the results showed that LPJ-GUESS using the extended phenological module substantially improved in the accuracy of spring and autumn phenology compared to the original phenological module. Furthermore, we found that differences in phenological estimations can have non-negligible effects on carbon and water cycling processes by influencing plant annual growth dynamics and ecosystem structure functions. For the carbon cycle, the influence of phenological differences on BNS- and Shrubs-dominated regions was greater than that of IBS&TeBS-dominated regions, and there were differences in the seasonality of monthly GPP simulations with different PFTs. For the water cycle, the AET simulations get higher in spring and get lower in summer, and only in the Shrubs-dominated region, the AET simulation get lower in autumn when the original phenology module is used. We highlighted the importance of phenology estimation and its process interactions in DGVMs and proposed further developments in vegetation phenology modelling to improve the accuracy of DGVM models in simulating the phenological dynamics and terrestrial carbon and water cycles.

Code and data availability

LPJ-GUESS is tested, refined, and developed by a global research community, but the model code is managed and maintained by the Department of Physical Geography and Ecosystem Science, Lund University, Sweden. The code version used for this study is stored in a central code repository and can be downloaded from https://doi.org/10.5281/zenodo.10416649. Additional details can be obtained by contacting the corresponding author. Details of relevant driving data and comparison data can be obtained from the data description section in this paper.

Declaration of Competing Interest

The authors declare that there are no known competing financial interests or personal relationships that influenced the work reported in this paper.

Acknowledgments

This study was supported by the International Cooperation and Exchanges NSFC-STINT (42111530181), the Distinguished Young Scholars (42025101) and the 111 Project (B18006). J.T. is supported by Villum Young Investigator (Grant No. VIL53048), Swedish FORMAS (Forskningsråd för hållbar utveckling) mobility Grant (2016-01580) Lund University strategic research area MERGE and European Union's Horizon 2020 research and innovation programme under Marie Sklodowska-Curie (Grant 707187). S.C., J.T. and Y.H.F. thank the Joint China-Sweden Mobility Program (Grant No. CH2020-8656). We appreciate the reviewers' constructive comments and

helpful suggestions.

Author contributions

YHF and JT conceived the ideas and designed the methodology; JT provided the modelling help for the LPJ-GUESS and participated in result interpretation and writing; SZC modified LPJ-GUESS according to the scheme design and analyzed the data, and YHF led the writing of the manuscript in corporation with SZC and JT; All authors contributed critically to the drafts and gave final approval for publication.

Reference

Ahl, D. E., Gower, S. T., Burrows, S. N., Shabanov, N. V., Myneni, R. B., and Knyazikhin, Y.: Monitoring spring canopy phenology of a deciduous broadleaf forest using MODIS, Remote Sensing of Environment, 104, 88-95, 2006.

Ahlström, A., Xia, J., Arneth, A., Luo, Y., and Smith, B.: Importance of vegetation dynamics for future terrestrial carbon cycling, Environmental Research Letters, 10, 054019, 2015.

Augspurger, C. K.: Spring 2007 warmth and frost: phenology, damage and refoliation in a temperate deciduous forest, Funct. Ecol., 23, 1031-1039, 2009.

Badeck, F. W., Bondeau, A., Böttcher, K., Doktor, D., Lucht, W., Schaber, J., and Sitch, S.: Responses of spring phenology to climate change, New Phytol., 162, 295-309, 2004.

Bartholome, E. and Belward, A. S.: GLC2000: a new approach to global land cover mapping from Earth observation data, Int. J. Remote Sens., 26, 1959-1977, 2005.

Bigler, C. and Bugmann, H.: Climate-induced shifts in leaf unfolding and frost risk of European trees and shrubs, Sci. Rep., 8, 9865, 2018.

Caffarra, A., Donnelly, A., and Chuine, I.: Modelling the timing of Betula pubescens budburst. II. Integrating complex effects of photoperiod into process-based models, Climate research, 46, 159-170, 2011.

Cao, S., Li, M., Zhu, Z., Zha, J., Zhao, W., Duanmu, Z., Chen, J., Zheng, Y., and Chen, Y.: Spatiotemporally consistent global dataset of the GIMMS Leaf Area Index (GIMMS LAI4g) from 1982 to 2020, Earth System Science Data Discussions, 1-31, 2023.

Chen, S., Fu, Y. H., Hao, F., Li, X., Zhou, S., Liu, C., and Tang, J.: Vegetation phenology and its ecohydrological implications from individual to global scales, Geography and Sustainability, 2022a.

Chen, S., Fu, Y. H., Geng, X., Hao, Z., Tang, J., Zhang, X., Xu, Z., and Hao, F.: Influences of Shifted Vegetation Phenology on Runoff Across a Hydroclimatic Gradient, Front. Plant Sci., 12, 802664, 10.3389/fpls.2021.802664, 2022b.

Chen, S., Fu, Y. H., Wu, Z., Hao, F., Hao, Z., Guo, Y., Geng, X., Li, X., Zhang, X., and Tang, J.: Informing the SWAT model with remote sensing detected vegetation phenology for improved modeling of ecohydrological processes, Journal of Hydrology, 616, 128817, 2023.

Chen, X., Wang, D., Chen, J., Wang, C., and Shen, M.: The mixed pixel effect in land surface phenology: A simulation study, Remote Sensing of Environment, 211, 338-344, 2018.

Chuine, I.: A unified model for budburst of trees, Journal of theoretical biology, 207, 337-347, 2000.

Chuine, I.: Why does phenology drive species distribution?, Philosophical Transactions of the Royal Society B: Biological Sciences, 365, 3149-3160, 2010.

Cong, N., Piao, S., Chen, A., Wang, X., Lin, X., Chen, S., Han, S., Zhou, G., and Zhang, X.: Spring vegetation green-up date in China inferred from SPOT NDVI data: A multiple model analysis, Agric. For. Meteorol., 165, 104-113, 10.1016/j.agrformet.2012.06.009, 2012.

Dai, W., Jin, H., Zhou, L., Liu, T., Zhang, Y., Zhou, Z., Fu, Y. H., and Jin, G.: Testing machine learning algorithms on a binary classification phenological model, Global Ecology and Biogeography, 32, 178-190, 2023.

Delpierre, N., Dufrêne, E., Soudani, K., Ulrich, E., Cecchini, S., Boé, J., and François, C.: Modelling interannual and spatial variability of leaf senescence for three deciduous tree species in France, Agric. For. Meteorol., 149, 938-948, 2009.

Deng, F., Chen, J. M., Plummer, S., Chen, M., and Pisek, J.: Algorithm for global leaf area index retrieval

using satellite imagery, IEEE Trans. Geosci. Remote Sens., 44, 2219-2229, 2006.
Dijkstra, J. A., Westerman, E. L., and Harris, L. G.: The effects of climate change on species composition, succession and phenology: a case study, Global Change Biol., 17, 2360-2369, 2011.
Drepper, B., Gobin, A., and Van Orshoven, J.: Spatio-temporal assessment of frost risks during the flowering of pear trees in Belgium for 1971–2068, Agric. For. Meteorol., 315, 108822, 2022.
Fang, J. and Lechowicz, M. J.: Climatic limits for the present distribution of beech (Fagus L.) species in the world, J. Biogeogr., 33, 1804-1819, 2006.
Forrest, J., Inouye, D. W., and Thomson, J. D.: Flowering phenology in subalpine meadows: Does climate variation influence community co-flowering patterns?, Ecology, 91, 431-440, 2010.
Fu, Y., Li, X., Zhou, X., Geng, X., Guo, Y., and Zhang, Y.: Progress in plant phenology modeling under global climate change, Science China Earth Sciences, 63, 1237-1247, 2020.
Fu, Y. H., Piao, S., Op de Beeck, M., Cong, N., Zhao, H., Zhang, Y., Menzel, A., and Janssens, I. A.: Recent spring phenology shifts in western C entral E urope based on multiscale observations, Global Ecol. Biogeogr., 23, 1255-1263, 2014.
Fu, Y. H., Geng, X., Chen, S., Wu, H., Hao, F., Zhang, X., Wu, Z., Zhang, J., Tang, J., and Vitasse, Y.: Global warming is increasing the discrepancy between green (actual) and thermal (potential) seasons of temperate trees, Global Change Biology, 29, 1377-1389, 2023.
Fu, Y. H., Li, X., Chen, S., Wu, Z., Su, J., Li, X., Li, S., Zhang, J., Tang, J., and Xiao, J.: Soil moisture regulates warming responses of autumn photosynthetic transition dates in subtropical forests, Global Change Biol., 28, 4935-4946, 2022.
Fu, Y. H., Zhou, X., Li, X., Zhang, Y., Geng, X., Hao, F., Zhang, X., Hanninen, H., Guo, Y., and De Boeck, H. J.: Decreasing control of precipitation on grassland spring phenology in temperate China, Global Ecol. Biogeogr., 30, 490-499, 2021.
Geng, X., Zhou, X., Yin, G., Hao, F., Zhang, X., Hao, Z., Singh, V. P., and Fu, Y. H.: Extended growing season reduced river runoff in Luanhe River basin, Journal of Hydrology, 582, 124538, 2020.
Guan, K., Pan, M., Li, H., Wolf, A., Wu, J., Medvigy, D., Caylor, K. K., Sheffield, J., Wood, E. F., and Malhi, Y.: Photosynthetic seasonality of global tropical forests constrained by hydroclimate, Nat. Geosci., 8, 284-289, 2015.
Hänninen, H.: Modelling bud dormancy release in trees from cool and temperate regions, 1990.
Hickler, T., Smith, B., Sykes, M. T., Davis, M. B., Sugita, S., and Walker, K.: Using a generalized vegetation model to simulate vegetation dynamics in northeastern USA, Ecology, 85, 519-530, 2004.
Hmimina, G., Dufrêne, E., Pontailler, J.-Y., Delpierre, N., Aubinet, M., Caquet, B., De Grandcourt, A., Burban, B., Flechard, C., and Granier, A.: Evaluation of the potential of MODIS satellite data to predict vegetation phenology in different biomes: An investigation using ground-based NDVI measurements, Remote Sens. Environ., 132, 145-158, 2013.
Huang, M., Piao, S., Janssens, I. A., Zhu, Z., Wang, T., Wu, D., Ciais, P., Myneni, R. B., Peaucelle, M., and Peng, S.: Velocity of change in vegetation productivity over northern high latitudes, Nat. Ecol. Evol., 1, 1649-1654, 2017.
Jain, A. K. and Yang, X.: Modeling the effects of two different land cover change data sets on the carbon stocks of plants and soils in concert with CO2 and climate change, Global Biogeochem. Cycles, 19, 2005.
Kaufmann, R. K., Zhou, L., Knyazikhin, Y., Shabanov, V., Myneni, R. B., and Tucker, C. J.: Effect of orbital drift and sensor changes on the time series of AVHRR vegetation index data, IEEE Trans. Geosci. Remote Sens., 38, 2584-2597, 2000.
Keenan, T. F. and Richardson, A. D.: The timing of autumn senescence is affected by the timing of spring

669 phenology: implications for predictive models, Global Change Biol., 21, 2634-2641, 2015.
670 Keenan, T. F., Gray, J., Friedl, M. A., Toomey, M., Bohrer, G., Hollinger, D. Y., Munger, J. W., O'Keefe,
671 J., Schmid, H. P., SueWing, I., Yang, B., and Richardson, A. D.: Net carbon uptake has increased through
672 warming-induced changes in temperate forest phenology, Nat. Clim. Change, 4, 598-604,
673 10.1038/Nclimate2253, 2014.
674 Kim, J. H., Hwang, T., Yang, Y., Schaaf, C. L., Boose, E., and Munger, J. W.: Warming-induced earlier
675 greenup leads to reduced stream discharge in a temperate mixed forest catchment, J. Geophys. Res.:
676 Biogeosci., 123, 1960-1975, 2018.
677 Kramer, K.: Selecting a model to predict the onset of growth of Fagus sylvatica, J. Appl. Ecol., 172-181,
678 1994.
679 Krinner, G., Viovy, N., de Noblet-Ducoudré, N., Ogée, J., Polcher, J., Friedlingstein, P., Ciais, P., Sitch,
680 S., and Prentice, I. C.: A dynamic global vegetation model for studies of the coupled atmosphere-
681 biosphere system, Global Biogeochem. Cycles, 19, 2005.
682 Kucharik, C. J., Barford, C. C., El Maayar, M., Wofsy, S. C., Monson, R. K., and Baldocchi, D. D.: A
683 multiyear evaluation of a Dynamic Global Vegetation Model at three AmeriFlux forest sites: Vegetation
684 structure, phenology, soil temperature, and CO2 and H2O vapor exchange, Ecol. Modell., 196, 1-31,
685 2006.
686 Li, X., Fu, Y. H., Chen, S., Xiao, J., Yin, G., Li, X., Zhang, X., Geng, X., Wu, Z., and Zhou, X.: Increasing
687 importance of precipitation in spring phenology with decreasing latitudes in subtropical forest area in
688 China, Agricultural and Forest Meteorology, 304, 108427, 2021.
689 Liu, Q., Fu, Y. H., Liu, Y., Janssens, I. A., and Piao, S.: Simulating the onset of spring vegetation growth
690 across the Northern Hemisphere, Global Change Biol., 24, 1342-1356, 2018a.
691 Liu, Q., Piao, S., Janssens, I. A., Fu, Y., Peng, S., Lian, X., Ciais, P., Myneni, R. B., Peñuelas, J., and
692 Wang, T.: Extension of the growing season increases vegetation exposure to frost, Nature
693 communications, 9, 426, 2018b.
694 Lu, J., Wang, G., Chen, T., Li, S., Hagan, D. F. T., Kattel, G., Peng, J., Jiang, T., and Su, B.: A harmonized
695 global land evaporation dataset from model-based products covering 1980–2017, Earth Syst. Sci. Data,
696 13, 5879-5898, 2021.
697 Marini, F. and Walczak, B.: Particle swarm optimization (PSO). A tutorial, Chemometrics and Intelligent
698 Laboratory Systems, 149, 153-165, 2015.
699 Medvigy, D., Wofsy, S., Munger, J., Hollinger, D., and Moorcroft, P.: Mechanistic scaling of ecosystem
700 function and dynamics in space and time: Ecosystem Demography model version 2, J. Geophys. Res.:
701 Biogeosci., 114, 2009.
702 Morales, P., Sykes, M. T., Prentice, I. C., Smith, P., Smith, B., Bugmann, H., Zierl, B., Friedlingstein, P.,
703 Viovy, N., and Sabaté, S.: Comparing and evaluating process-based ecosystem model predictions of
704 carbon and water fluxes in major European forest biomes, Global change biology, 11, 2211-2233, 2005.
705 Morisette, J. T., Richardson, A. D., Knapp, A. K., Fisher, J. I., Graham, E. A., Abatzoglou, J., Wilson, B.
706 E., Breshears, D. D., Henebry, G. M., and Hanes, J. M.: Tracking the rhythm of the seasons in the face
707 of global change: phenological research in the 21st century, Front. Ecol. Environ., 7, 253-260, 2009.
708 Piao, S., Fang, J., Zhou, L., Ciais, P., and Zhu, B.: Variations in satellite-derived phenology in China's
709 temperate vegetation, Global Change Biol., 12, 672-685, 2006.
710 Piao, S., Liu, Q., Chen, A., Janssens, I. A., Fu, Y., Dai, J., Liu, L., Lian, X., Shen, M., and Zhu, X.: Plant
711 phenology and global climate change: Current progresses and challenges, Global change biology, 25,
712 1922-1940, 2019.

Pinzon, J. E. and Tucker, C. J.: A non-stationary 1981–2012 AVHRR NDVI3g time series, Remote Sens., 6, 6929-6960, 2014.
Poli, R., Kennedy, J., and Blackwell, T.: Particle swarm optimization: An overview, Swarm Intell., 1, 33-57, 2007.
Prevéy, J., Vellend, M., Rüger, N., Hollister, R. D., Bjorkman, A. D., Myers-Smith, I. H., Elmendorf, S. C., Clark, K., Cooper, E. J., and Elberling, B.: Greater temperature sensitivity of plant phenology at colder sites: implications for convergence across northern latitudes, Global Change Biol., 23, 2660-2671, 2017.
Reed, B. C., Brown, J. F., VanderZee, D., Loveland, T. R., Merchant, J. W., and Ohlen, D. O.: Measuring phenological variability from satellite imagery, Journal of vegetation science, 5, 703-714, 1994.
Richardson, A. D., Anderson, R. S., Arain, M. A., Barr, A. G., Bohrer, G., Chen, G., Chen, J. M., Ciais, P., Davis, K. J., and Desai, A. R.: Terrestrial biosphere models need better representation of vegetation phenology: results from the N orth A merican C arbon P rogram S ite S ynthesis, Global Change Biology, 18, 566-584, 2012.
Rinnan, R., Iversen, L. L., Tang, J., Vedel-Petersen, I., Schollert, M., and Schurgers, G.: Separating direct and indirect effects of rising temperatures on biogenic volatile emissions in the Arctic, Proceedings of the National Academy of Sciences, 117, 32476-32483, 10.1073/pnas.2008901117, 2020.
Roberts, A. M., Tansey, C., Smithers, R. J., and Phillimore, A. B.: Predicting a change in the order of spring phenology in temperate forests, Global Change Biol., 21, 2603-2611, 2015.
Rollinson, C. R. and Kaye, M. W.: Experimental warming alters spring phenology of certain plant functional groups in an early successional forest community, Global Change Biol., 18, 1108-1116, 2012.
Ryu, S.-R., Chen, J., Noormets, A., Bresee, M. K., and Ollinger, S. V.: Comparisons between PnET-Day and eddy covariance based gross ecosystem production in two Northern Wisconsin forests, Agric. For. Meteorol., 148, 247-256, 2008.
Sarvas, R.: Investigations on the annual cycle of development of forest trees. Active period, Investigations on the annual cycle of development of forest trees. Active period., 76, 1972.
Savitzky, A. and Golay, M. J.: Smoothing and differentiation of data by simplified least squares procedures, Anal. Chem., 36, 1627-1639, 1964.
Schaefer, K., Collatz, G. J., Tans, P., Denning, A. S., Baker, I., Berry, J., Prihodko, L., Suits, N., and Philpott, A.: Combined simple biosphere/Carnegie-Ames-Stanford approach terrestrial carbon cycle model, J. Geophys. Res.: Biogeosci., 113, 2008.
Sellers, P., Mintz, Y., Sud, Y. e. a., and Dalcher, A.: A simple biosphere model (SiB) for use within general circulation models, J. Atmos. Sci., 43, 505-531, 1986.
Sellers, P., Randall, D., Collatz, G., Berry, J., Field, C., Dazlich, D., Zhang, C., Collelo, G., and Bounoua, L.: A revised land surface parameterization (SiB2) for atmospheric GCMs. Part I: Model formulation, J. Clim., 9, 676-705, 1996.
Sitch, S., Smith, B., Prentice, I. C., Arneth, A., Bondeau, A., Cramer, W., Kaplan, J. O., Levis, S., Lucht, W., and Sykes, M. T.: Evaluation of ecosystem dynamics, plant geography and terrestrial carbon cycling in the LPJ dynamic global vegetation model, Global Change Biol., 9, 161-185, 2003.
Smith, B., Prentice, I. C., and Sykes, M. T.: Representation of vegetation dynamics in the modelling of terrestrial ecosystems: comparing two contrasting approaches within European climate space, Global ecology and biogeography, 621-637, 2001.
Sykes, M. T., Prentice, I. C., and Cramer, W.: A bioclimatic model for the potential distributions of north European tree species under present and future climates, Journal of Biogeography, 203-233, 1996.

Tang, J., Zhou, P., Miller, P. A., Schurgers, G., Gustafson, A., Makkonen, R., Fu, Y. H., and Rinnan, R.: High-latitude vegetation changes will determine future plant volatile impacts on atmospheric organic aerosols, npj Climate and Atmospheric Science, 6, 147, 2023.

Thornton, P. E., Law, B. E., Gholz, H. L., Clark, K. L., Falge, E., Ellsworth, D. S., Goldstein, A. H., Monson, R. K., Hollinger, D., and Falk, M.: Modeling and measuring the effects of disturbance history and climate on carbon and water budgets in evergreen needleleaf forests, Agric. For. Meteorol., 113, 185-222, 2002.

Tremblay, N. O. and Larocque, G. R.: Seasonal dynamics of understory vegetation in four eastern Canadian forest types, International Journal of Plant Sciences, 162, 271-286, 2001.

Tucker, C. J., Pinzon, J. E., Brown, M. E., Slayback, D. A., Pak, E. W., Mahoney, R., Vermote, E. F., and El Saleous, N.: An extended AVHRR 8-km NDVI dataset compatible with MODIS and SPOT vegetation NDVI data, Int. J. Remote Sens., 26, 4485-4498, 2005.

Viovy, N.: CRUNCEP version 7-atmospheric forcing data for the community land model, 2018.

White, M. A., Thornton, P. E., and Running, S. W.: A continental phenology model for monitoring vegetation responses to interannual climatic variability, Global Biogeochem. Cycles, 11, 217-234, 1997.

White, M. A., de Beurs, K. M., Didan, K., Inouye, D. W., Richardson, A. D., Jensen, O. P., O'keefe, J., Zhang, G., Nemani, R. R., and van Leeuwen, W. J.: Intercomparison, interpretation, and assessment of spring phenology in North America estimated from remote sensing for 1982–2006, Global Change Biology, 15, 2335-2359, 2009.

Wolkovich, E. M., Cook, B. I., Allen, J. M., Crimmins, T., Betancourt, J. L., Travers, S. E., Pau, S., Regetz, J., Davies, T. J., and Kraft, N. J.: Warming experiments underpredict plant phenological responses to climate change, Nature, 485, 494-497, 2012.

Zani, D., Crowther, T. W., Mo, L., Renner, S. S., and Zohner, C. M.: Increased growing-season productivity drives earlier autumn leaf senescence in temperate trees, Science, 370, 1066-1071, 2020.

Zhang, Y., Commane, R., Zhou, S., Williams, A. P., and Gentine, P.: Light limitation regulates the response of autumn terrestrial carbon uptake to warming, Nat. Clim. Change, 10, 739-743, 2020.

Zhang, Y., Xiao, X., Wu, X., Zhou, S., Zhang, G., Qin, Y., and Dong, J.: A global moderate resolution dataset of gross primary production of vegetation for 2000–2016, Sci. Data, 4, 1-13, 2017.

Zheng, J., Jia, G., and Xu, X.: Earlier snowmelt predominates advanced spring vegetation greenup in Alaska, Agricultural and Forest Meteorology, 315, 108828, 2022.

Zhou, X., Geng, X., Yin, G., Hänninen, H., Hao, F., Zhang, X., and Fu, Y. H.: Legacy effect of spring phenology on vegetation growth in temperate China, Agricultural and Forest Meteorology, 281, 107845, 2020.

Zhu, Z., Piao, S., Myneni, R. B., Huang, M., Zeng, Z., Canadell, J. G., Ciais, P., Sitch, S., Friedlingstein, P., and Arneth, A.: Greening of the Earth and its drivers, Nat. Clim. Change, 6, 791-795, 2016.

Zohner, C. M., Mirzagholi, L., Renner, S. S., Mo, L., Rebindaine, D., Bucher, R., Palouš, D., Vitasse, Y., Fu, Y. H., and Stocker, B. D.: Effect of climate warming on the timing of autumn leaf senescence reverses after the summer solstice, Science, 381, eadf5098, 2023.